Synthesis, composition optimization, and tunable red emission of $CaAlSiN_3:Eu^{2+}$ phosphors for white light-emitting diodes

Shu-Xing Li
The State Key Lab of High Performance Ceramics and Superfine Microstructure, Shanghai Institute of Ceramics, Chinese Academy of Sciences, Shanghai 200050, China; and University of Chinese Academy of Sciences, Beijing 100049, China

Xue-Jian Liu[a)]
The State Key Lab of High Performance Ceramics and Superfine Microstructure, Shanghai Institute of Ceramics, Chinese Academy of Sciences, Shanghai 200050, China

Jia-Qing Liu and Huili Li
Engineering Research Center for Nanophotonics and Advanced Instrument, Ministry of Education, Department of Physics, East China Normal University, Shanghai 200062, China

Ri-Hua Mao
Analysis and Testing Center for Inorganic Materials, Shanghai Institute of Ceramics, Chinese Academy of Sciences, Shanghai 200050, China

Zheng-Ren Huang
The State Key Lab of High Performance Ceramics and Superfine Microstructure, Shanghai Institute of Ceramics, Chinese Academy of Sciences, Shanghai 200050, China

Rong-Jun Xie[b),c)]
Sialon Group, Sialon Unit, National Institute for Materials Science (NIMS), Namiki 1-1, Tsukuba, Ibaraki 305-0044, Japan

(Received 15 February 2015; accepted 20 April 2015)

$Ca_{0.98}Eu_{0.02}Al_{1-4\delta/3}Si_{1+\delta}N_3$ (δ = 0–0.36) red-emitting phosphors were prepared by carbothermal reduction and nitridation method with stable and inexpensive $CaCO_3$ as Ca source. Optimal nominal composition was obtained at δ = 0.18, showing intense emission peaked at 625 nm and high external quantum efficiency of 71%. The emission wave length could be successfully tuned from 630 to 606 nm with increasing δ value. $Ca_{0.98}Eu_{0.02}Al_{1-4\delta/3}Si_{1+\delta}N_3$ phosphors provided two coordinated environments for Eu^{2+} ions, resulting in two fitted Gaussian peaks. Energy transfer from Eu^{2+} sites in Si-rich environments to those in Si/Al-equivalent modes has been confirmed by analysis of the decay curve of each peak. The decay behaviors suggested that energy transfer effect slowed with higher δ value. Finally, warm white light was created by combining as-prepared red-emitting $Ca_{0.98}Eu_{0.02}Al_{0.76}Si_{1.18}N_3$ and yellow-emitting $YAG:Ce^{3+}$ phosphors with a blue-emitting chip, exhibiting a color rendering index R_a of 91 at a low correlated color temperature of 3500 K with a luminous efficiency of 79 lm/W.

I. INTRODUCTION

In recent years, light-emitting diodes (LEDs) have attracted considerable interest owing to their superior properties such as high efficiency, low-voltage driving, long lifetime, great reliability, and environmental friendliness.[1–3] Most commercially available white LEDs are fabricated by combining blue-emitting LED chips (440–470 nm) with $YAG:Ce^{3+}$ yellow-emitting phosphor materials, but they show drawbacks of low color rendering index (CRI < 75) and high correlated color temperature (CCT > 4500 K) due to lack of red component in the spectral region.[4–6] However, this issue can be improved by a slight addition of red-emitting phosphors with high luminescent efficiency to $YAG:Ce^{3+}$.[7] To this end, great efforts have been made to exploit novel red phosphors, and the most successful materials are rare-earth-doped (oxy)nitride compounds. Most currently, red-emitting nitride phosphors include $M_2Si_5N_8:Eu^{2+}$ (M = Ca, Sr, Ba),[8–14] $CaAlSiN_3:Eu^{2+}$,[15–21] and $Sr[LiAl_3N_4]:Eu^{2+}$.[22] Among them, $CaAlSiN_3:Eu^{2+}$ red-emitting phosphor materials have received great attention for excellent color rendition (CRI > 90) white LED because of many favorable

Contributing Editor: Zoltan Lences
Address all correspondence to these authors.
[a)]e-mail: xjliu@mail.sic.ac.cn
[b)]e-mail: XIE.Rong-Jun@nims.go.jp
[c)]This author was an editor of this focus issue the review and decision stage. For the *JMR* policy on review and publication of manuscripts authored by editors, please refer to http://www.mrs.org/jmr-editor-manuscripts/
DOI: 10.1557/jmr.2015.125

 © Materials Research Society 2015

https://doi.org/10.1557/jmr.2015.125 Published online by Cambridge University Press

luminescent properties, such as high quantum efficiency, excellent thermal property, and chemical stability.

Despite these significant advantages, it is also found that the emission peaks of $CaAlSiN_3:Eu^{2+}$ are mostly beyond 650 nm and can hardly meet the required wavelengths (about 620 nm) of high luminous efficiency white LEDs due to effects of relatively sensitive function of human visual system. An effective choice is to develop cationic/anionic substitution method to modify the photoluminescence properties of the phosphors. A notable example is $YAG:Ce^{3+}$ phosphors that the emission band can be blue or red shifted by partial replacement of Al with Ga or of Y with Gd. Systematic substitutional effects on the photoluminescence by substituting AlO^+ for SiN^+ in the $M_2Si_5N_8$ family to create $M_2Si_{5-x}Al_xN_{8-x}O_x$ have also been reported.[14] As for $CaAlSiN_3$ family, Watanabe and Kijima[23] have introduced Sr^{2+} to replace Ca^{2+} under an unapproachable pressure of 190 MPa to expand the crystal lattice and weaken the crystal field strength around Eu^{2+}, leading to the blueshift of emission maxima from 650 to 610 nm. Wang et al.[24] have demonstrated that emission peaks of $CaAlSiN_3$-type phosphors can be tuned from 650 to 610 nm by oxygen substitutions for nitrogen at the sacrifice of quantum efficiency. Consequently, new methods should be developed to realize the blue-shift emission.

On the other hand, common preparation for $CaAlSiN_3:Eu^{2+}$ phosphors was limited due to expensive and air-sensitive raw materials, e.g., Ca_3N_2 and EuN. Traditional solid-state reaction with a powder mixture of Ca_3N_2, EuN, AlN, and Si_3N_4 as raw materials required critical conditions of high temperature up to 1800 °C and high pressure more than 0.9 MPa to produce high quality powders with good crystallinity.[15] As an alternative, $CaAlSiN_3:Eu^{2+}$ was synthesized via self-propagating high-temperature synthesis with (Ca, Eu)AlSi alloy in a radio-frequency furnace.[17] However, the evaporation of Ca and Al metals during the arc-melting led to difficulty in exact control of the product performance. Li et al.[16] reported the synthesis of $CaAlSiN_3:Eu^{2+}$ by nitridation of (Ca, Eu) AlSi alloy in supercritical ammonia (100 MPa) with low yield. Recently, Suehiro et al.[21] reported the synthesis of $CaAlSiN_3:Eu^{2+}$ by gas reduction nitridation method with $CaO–Al_2O_3–SiO_2$ at the narrow temperature range of 1365–1375 °C, leading to insufficient nitridation reaction due to low eutectic melting of the reaction system. To overcome the challenges of the aforementioned preparation processes, carbothermal reduction and nitridation (CTRN) method with stable and common $CaCO_3$ as Ca source has been successfully applied for the facile synthesis of $CaAlSiN_3:Eu^{2+}$ in our previous research.[25] Besides, AlN-like secondary phase was always formed according to the stoichiometric composition with a Ca/Al/Si molar ratio of 1:1:1 to prepare $CaAlSiN_3$-based red-emitting phosphors even at high temperature and pressure because of the low solubility of Al in $CaAlSiN_3$. Li et al.[18] proposed a formula of $CaAl_{1-4\delta/3}Si_{1+\delta}N_3$ ($\delta \approx 0.3–0.4$) with an Al/Si molar ratio of about 1:2 instead of the ideal 1:1 according to bond valence sum calculations of $CaAlSiN_3$. However, the optimal δ value remains unclear till now.

In this present research, the CTRN method is applied to synthesize $CaAl_{1-4\delta/3}Si_{1+\delta}N_3:Eu^{2+}$ ($\delta = 0–0.36$) series red-emitting phosphors. The influences of Si/Al molar ratio on phase compositions and the emission spectra are reported in detail. The emission spectra have been blue shifted by increasing the Si/Al molar ratio. The origin of the two Gaussian components that constitute the emission spectra has been identified. Active site-to-site energy transfer mechanism from the Eu^{2+} activator sites in the Si-rich environments to those in the Si/Al-equivalent environments has been clarified by examining the time-resolved photoluminescence (TRPL) and decay curves. At the same time, warm white LEDs with high color rendition have been fabricated by the addition of as-prepared red-emitting phosphors.

II. EXPERIMENTAL

Nominal compositions of $Ca_{0.98}Eu_{0.02}Al_{1-4\delta/3}Si_{1+\delta}N_3$ ($\delta = 0–0.36$) red-emitting phosphors were successfully prepared from $CaCO_3$ (99.99%), AlN (Tokuyama, H-Grade), α-Si_3N_4 (UBE, E-10), Eu_2O_3 (99.99%), and C powder (99.95%). Excess carbon as a reducing agent in a C/O ratio of 1.5:1 was added to ensure the reduction of CaO ($CaCO_3$ was decomposed completely into CaO at high temperature) and Eu_2O_3 to achieve a low oxygen content in the final products. Approximately 6.2 g of raw powders were thoroughly mixed and loaded into a molybdenum boat (length = 55 mm, width = 35 mm, depth of the powder bed ≈ 7 mm) in a horizontal tube furnace (inner diameter of 60 mm) for two-step heating after the vacuuming process, which was first carried out to the degree of −0.1 MPa, then repeated the process for another two times after filling the tube cavity with pure nitrogen. First, the mixture was heated in N_2 with a constant flow rate of 200 mL min^{-1} at 850 °C for 1 h to decompose $CaCO_3$ completely. Then, the temperature was increased to 1600 °C and maintained for 4 h in 200 mL min^{-1} N_2–20 mL min^{-1} H_2 gas mixture to form the nitrides and complete the reduction of Eu^{3+} to Eu^{2+}. After that, the fired samples were ground finely for measurements. It is unnecessary to remove residual unreacted carbon by post heat-treatment because the carbon content keeps below 0.5 wt% for the as-prepared products.

The phase compositions were determined by x-ray diffraction (XRD, Bruker D8 Advanced, Bruker AXS GMBH, Beijing, China) with Cu $K_{\alpha 1}$ radiation ($\lambda = 0.15406$ nm) at 40 kV and 40 mA. A step size of 0.02° was used with a scan speed of 5°/min. The lattice parameters were obtained by refining XRD patterns using

https://doi.org/10.1557/jmr.2015.125 Published online by Cambridge University Press

software package of Fullprof Suite. The cationic compositions of the samples were analyzed by inductively coupled plasma atomic emission spectrometry (ICP-AES, Vista AX, Varian). The nitrogen and oxygen contents of the synthesized powders were determined by O and N analyzers (TC600C, LECO Instrument LD), and the impurity carbon contents were performed using a C measurement device (SICMMC-222), respectively. The photoluminescence spectra and quantum yield were measured by a fluorescence spectrophotometer (Jobin Yvon, Fluoromax-4, Horiba Jobin Yvon, Paris, France) with a 150 W Xe lamp. The quantum efficiency was estimated using an integrating sphere unit (Jobin Yvon, F-3029) with a monochromatic source of 460 nm. The TRPL spectra and decay curves at room temperature were measured using an Edinburgh FLS980 Fluorescence Spectrophotometer with an excitation wave length of 460 nm. The optical properties of the as-fabricated white LEDs were investigated by a UV–VIS-near IR Spectrophotocolorimeter (PMS-80) with an output power of 1 W at room temperature.

III. RESULTS AND DISCUSSION

Figure 1 shows the typical XRD patterns of as-prepared $Ca_{0.98}Eu_{0.02}Al_{1-4\delta/3}Si_{1+\delta}N_3$ (δ = 0–0.36) powders. Samples exhibit various phase compositions for different δ values. In the range of $0 \le \delta \le 0.12$, besides $CaAlSiN_3$ main phase (ICSD#161796 for $CaAl_{0.54}Si_{1.38}N_3$),[16] there exists minor unreacted AlN phase. The content of AlN decreases with increasing δ value. However, an unknown phase appears for $0.24 \le \delta \le 0.36$. The study in progress suggests that the unknown phase is a Si-rich compound, and the result will be the subject of another publication. By contrast, no clear secondary phase is detected for the sample at $\delta = 0.18$. Nevertheless, the XRD peaks splitting around 32° and 37.5° with increasing δ value indicate that the structure is substantially distorted from the structure of $CaAlSiN_3$. According to the JCPDS card 39-0747, the samples are considered to be a solid solution of $CaAlSiN_3$ and Si_2N_2O.[26–28] Additionally, the severer peaks splitting with increasing δ value probably imply a tiny higher concentration of Si_2N_2O content in $CaAlSiN_3$–Si_2N_2O solid solution.

Figure 2 displays lattice parameters of *a*, *b*, and *c* with different δ values. The lattice parameters become significantly small with increasing δ value because of the shrinkage of host lattice caused by the short Si–N (1.65–1.75 Å) instead of long Al–N (1.75–1.85 Å).[18] On the other hand, the linear relationship between lattice parameters and δ values is observed with $0.12 \le \delta \le 0.24$, implying that it is more favorable to obtain $CaAlSiN_3$-based phase without impurities in the region of $0.12 \le \delta \le 0.24$.

Table I shows the analyzed cationic ratios of synthesized samples by ICP-AES for different nominal compositions. A Ca deficiency of about 20% is observed. It means that some amount of Ca component is evaporated at high temperature. Obviously, the charge imbalance caused by Ca^{2+} ion vacancy V_{Ca} is compensated by introduction of the substitutional oxygen O_N. The quantity ratios of Al and Si in the product largely coincide with the initial values. As presented in Table II, the mass fractions of N, O, and C in the as-prepared products rise a little because the formula weight of $Ca_{0.98}Eu_{0.02}Al_{1-4\delta/3}Si_{1+\delta}N_3$ decreases with increasing δ value. In addition, the very tiny increase of Si_2N_2O content in $CaAlSiN_3$–Si_2N_2O solid solution for rising δ value may also partially account for the small increment of O and C contents.

Figure 3 presents the photoluminescence spectra of $Ca_{0.98}Eu_{0.02}Al_{1-4\delta/3}Si_{1+\delta}N_3$ (δ = 0–0.36) phosphors. Obviously, all the samples display a broad absorption band from near-UV to yellow region (250–600 nm).

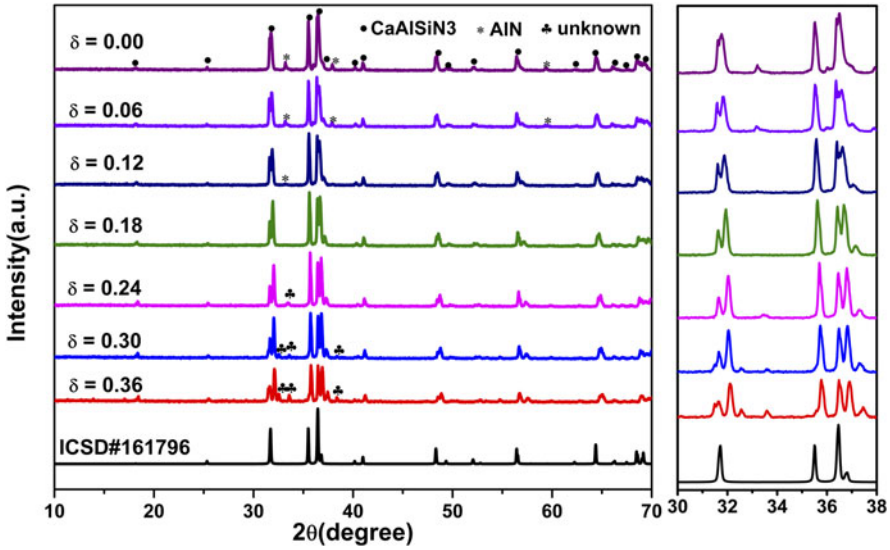


FIG. 1. XRD patterns of $Ca_{0.98}Eu_{0.02}Al_{1-4\delta/3}Si_{1+\delta}N_3$ (δ = 0–0.36) phosphors with various δ values.

https://doi.org/10.1557/jmr.2015.125 Published online by Cambridge University Press

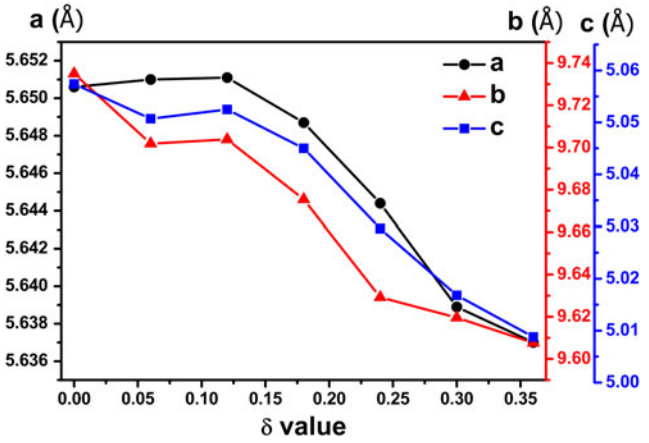


FIG. 2. Lattice parameters of $Ca_{0.98}Eu_{0.02}Al_{1-4\delta/3}Si_{1+\delta}N_3$ (δ = 0–0.36) phosphors with various δ values.

TABLE I. Analyzed cationic ratios of synthesized samples with different nominal compositions.

	Initial composition			Final composition[a]		
Sample	Ca	Al	Si	Ca	Al	Si
δ = 0.00	0.98	1.00	1.00	0.801(8)	1.035(0)	0.965(0)
δ = 0.06	0.98	0.92	1.06	0.778(4)	0.922(4)	1.057(6)
δ = 0.12	0.98	0.84	1.12	0.826(7)	0.858(2)	1.101(8)
δ = 0.18	0.98	0.76	1.18	0.806(8)	0.767(0)	1.173(0)
δ = 0.24	0.98	0.68	1.24	0.822(8)	0.707(9)	1.212(1)
δ = 0.30	0.98	0.60	1.30	0.789(9)	0.608(8)	1.291(2)
δ = 0.36	0.98	0.52	1.36	0.821(2)	0.533(9)	1.346(1)

[a]Normalized against the total Al + Si = 2−δ/3.

TABLE II. Measured mass fractions of N, O, and C and normalized N/O ratios of synthesized samples with different nominal compositions.

	Measured (%)			Normalized[b]	
Sample	N	O	C	N	O
δ = 0.00	23.12	1.39	0.15	2.829(9)	0.170(1)
δ = 0.06	23.96	1.54	0.16	2.818(8)	0.181(2)
δ = 0.12	23.71	1.36	0.17	2.837(3)	0.162(7)
δ = 0.18	24.32	1.67	0.21	2.807(2)	0.192(8)
δ = 0.24	24.22	1.70	0.23	2.803(2)	0.196(8)
δ = 0.30	25.25	1.69	0.30	2.811(8)	0.188(2)
δ = 0.36	24.43	1.82	0.44	2.792(0)	0.208(0)

[b]Normalized against the total N + O = 3.

Under the excitation of 460 nm, an intense red emission can be observed, which is attributed to the allowed $4f^6 5d^1 \rightarrow 4f^7$ transition of Eu^{2+} ions. The peaks of emission spectra gradually shift from 630 to 606 nm with δ value increasing from 0 to 0.36 despite the lattice contraction as shown in Fig. 4. It might suggest that the photoluminescence property is significantly correlated with the local environment of activators, which will be

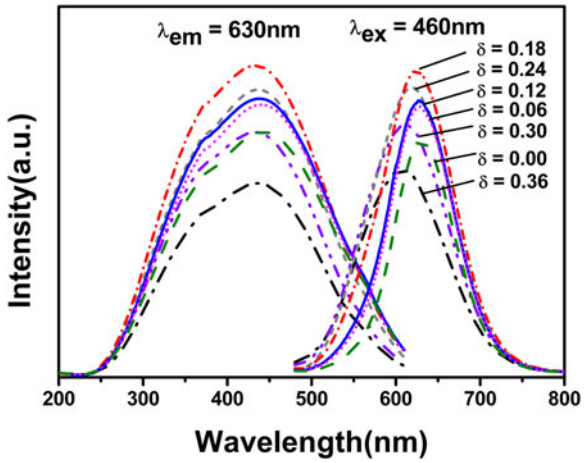


FIG. 3. Photoluminescence spectra of $Ca_{0.98}Eu_{0.02}Al_{1-4\delta/3}Si_{1+\delta}N_3$ (δ = 0–0.36) phosphors with various δ values.

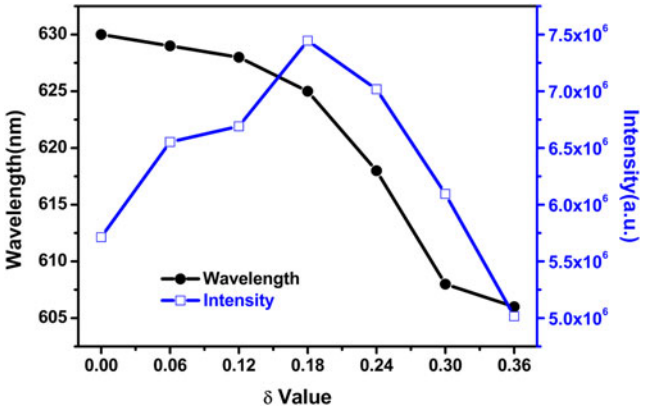


FIG. 4. Dependence of peak emission intensity and wave length on the δ value.

discussed in the following part. The luminescence intensity reaches the maximum at a δ value of 0.18 with external quantum efficiency up to 71% as a result of the higher phase purity, and the full width at half maximum (FWHM) is around 100 nm, which is close to the values (~88–105 nm) synthesized by other methods. Additionally, the emission intensity of $Ca_{0.98}Eu_{0.02}Al_{0.76}Si_{1.18}N_3$ phosphor at 250 °C remains 91% in comparison with the intensity at room temperature, suggesting low quenching property.

Although the existence of Si_2N_2O will contribute to the blueshift in emission,[28] the O contents suggest that there is extremely small concentration difference of Si_2N_2O for δ values from 0 to 0.36. Actually, the big changes of Al/Si contents for different δ values are mainly responsible for the blueshift from 630 to 606 nm. The observed blueshift in emission with higher Si/Al molar ratio can be elucidated from the variable covalence of the Eu^{2+} activator accommodation controlled by neighboring cations.[29] The Ca^{2+} cation is surrounded by coordinated nitrides that also have other branches connecting with

https://doi.org/10.1557/jmr.2015.125 Published online by Cambridge University Press

neighboring cations, e.g., Si^{4+}, Al^{3+}, and outer Ca^{2+} cations. The neighboring Al^{3+} cation at the second shell is substituted by Si^{4+} with increasing δ, creating Si-rich instead of Si/Al-equivalent environment. In the case of $\delta = 0$, Si-rich environments still exist because of the low solution of Al in $CaAlSiN_3$. The nitride anion connecting with a Si^{4+} cation would introduce more covalence than with an Al^{3+} cation, reflecting that the binding strength of Si–N is stronger than that of Al–N, therefore, gaining a longer and looser Ca–N. As the Eu^{2+} activator is introduced, it would preferably be accommodated at the looser Ca^{2+} site to minimize the lattice strain because the Eu^{2+} cation is larger than the Ca^{2+} cation. Thus, the covalent character and crystal field strength of the Eu^{2+} accommodations in Si-rich environment are weaker compared with Si/Al-equivalent environments. At the same time, Si-rich environments progressively increase with δ value, leading to the corresponding blue-shift emission.

TRPL spectra with fitted Gaussian deconvolution of $Ca_{0.98}Eu_{0.02}Al_{1-4\delta/3}Si_{1+\delta}N_3$ for $\delta = 0$ and 0.36 at two different delay times (100 and 1800 ns) are shown in Fig. 5. The emission spectra comprise two distinct emission peaks originating from Si-rich and Si/Al-equivalent environments,[30] respectively. The Eu^{2+} ions in Si-rich environments generate high-energy emission while those in Si/Al-equivalent environments lead to low-energy component. The high-energy component decreases gradually with an extension of delay time from 100 to 1800 ns. This is ascribed to the brisk energy transfer from Eu^{2+} ions in Si-rich environments to those in Si/Al-equivalent environments. In particular, for $\delta = 0$, the high-energy component almost disappears at the delay time of 1800 ns. By contrast, the high-energy component decreases only a little for $\delta = 0.36$. In the host of $\delta = 0.36$ with more Si^{4+} ions, more Eu^{2+} ions locate at the sites with Si-rich modes and less Eu^{2+} ions in Si/Al-equivalent environments. The formation of more Si-rich and less Si/Al-equivalent coordinated modes leads to a lowered chance for the energy transfer and results in a small decrease of high energy component eventually. This can be verified from the decay curves for $\delta = 0$ and 0.36 detected at 550 and 700 nm, as depicted in Fig. 6. The decay curves monitored at 550 and 700 nm stand for the decay behavior of high energy (Si-rich environment) and low energy (Si/Al-equivalent environment) components, respectively.

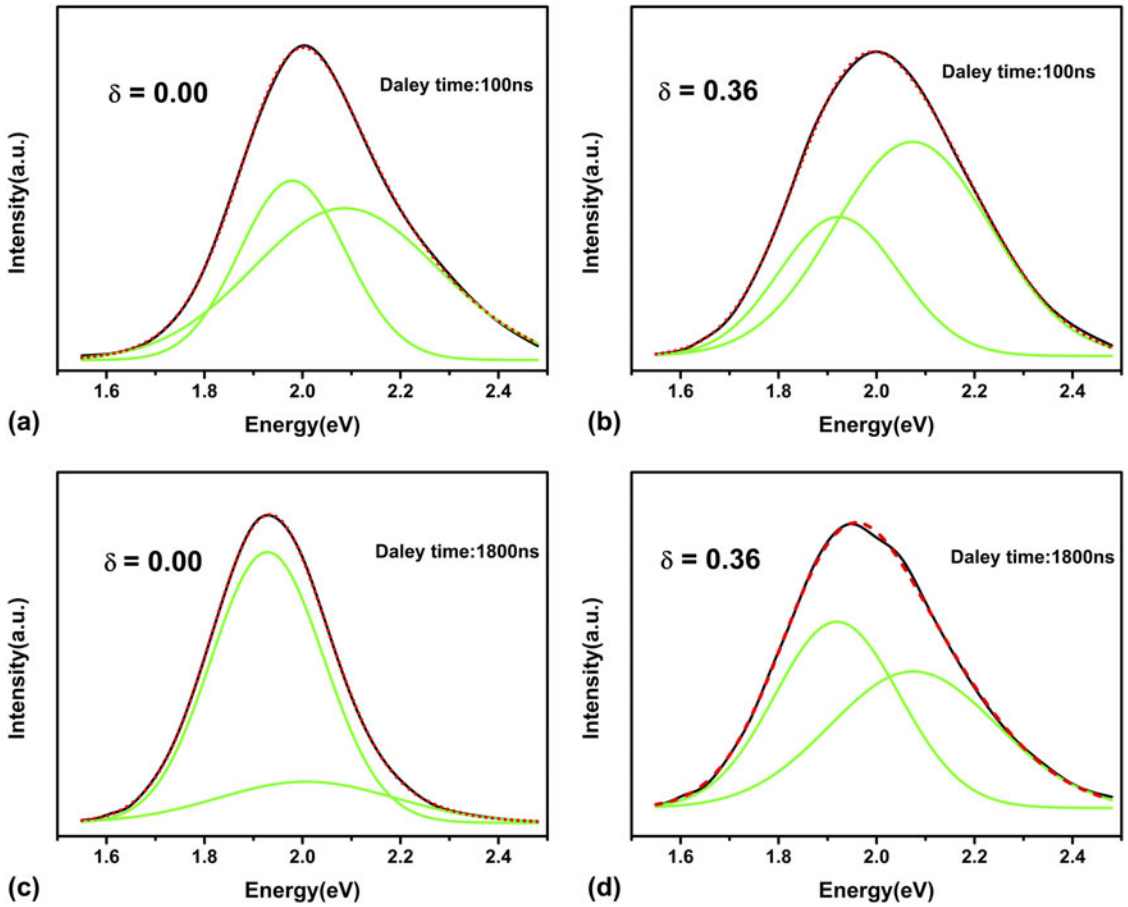


FIG. 5. TRPL spectra with fitted Gaussian deconvolution of $Ca_{0.98}Eu_{0.02}Al_{1-4\delta/3}Si_{1+\delta}N_3$ for $\delta = 0$ (a and c) and 0.36 (b and d).

https://doi.org/10.1557/jmr.2015.125 Published online by Cambridge University Press

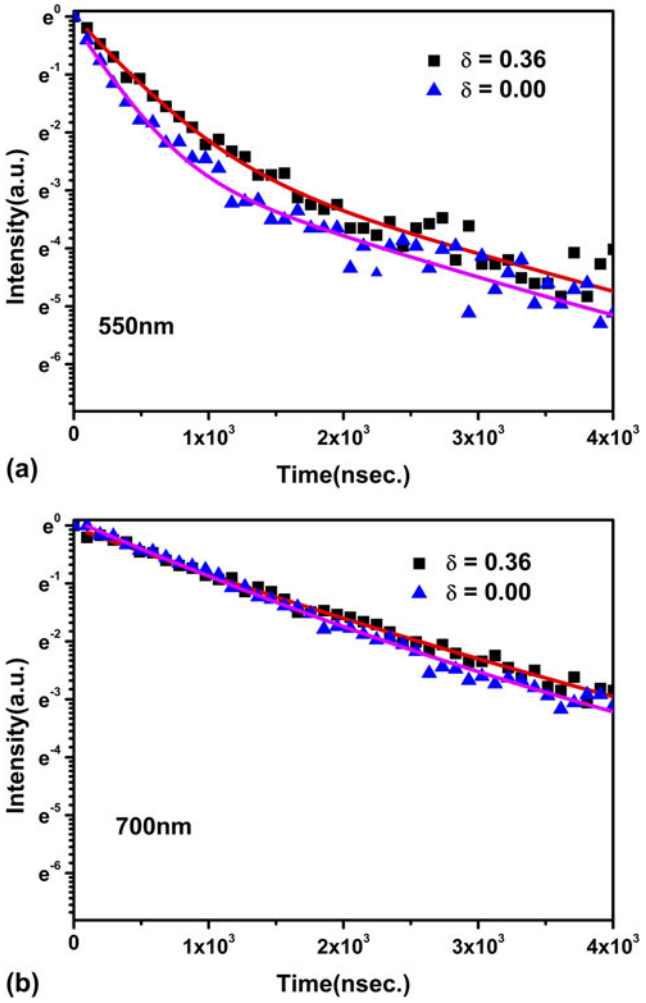


FIG. 6. Decay curves monitored at (a) 550 nm and (b) 700 nm for $Ca_{0.98}Eu_{0.02}Al_{1-4\delta/3}Si_{1+\delta}N_3$ with $\delta = 0$ and 0.36.

Both of the decay curves monitored at 550 nm show nonexponential form in Fig. 6(a), which is a typical sign of energy transfer.[31,32] The decay curves suggest that the lifetime of Eu^{2+} activators for $\delta = 0$ is a little shorter than that for $\delta = 0.36$. It is confirmed that the site-to-site energy transfer occurs more strongly for $\delta = 0$ than for $\delta = 0.36$. By contrast, the decay curves monitored at 700 nm exhibit almost coincident single-exponential decay lines, which means that the low energy components (Si/Al-equivalent environment) for $\delta = 0$ and 0.36 have the same decay rate. Both curves originate from the radiative decay of Eu^{2+} activators in Si/Al-equivalent environments. For the reason that the energy transfer never occurs between Eu^{2+} ions both in Si/Al-equivalent environments, the decay curve can be regarded as the typical radiative decay for Eu^{2+} ions accommodated in Si/Al-equivalent environments.

Figure 7 shows the TRPL spectra of $Ca_{0.98}Eu_{0.02}Al_{1-4\delta/3}Si_{1+\delta}N_3$ with $\delta = 0$–0.36. For all δ values, the energy transfer occurs sequentially from the high energy Eu^{2+} ions in the Si-rich environments to the low-energy Eu^{2+} ions in the Si/Al-equivalent environments and leads to the decline of high-energy emission and the simultaneous increasing of low-energy emission. The active energy transfer eventually controls the final spectral distribution.

Commission Internationale de l'Eclairage (CIE) chromaticity coordinates for $Ca_{0.98}Eu_{0.02}Al_{1-4\delta/3}Si_{1+\delta}N_3$ ($\delta = 0$–0.36) are presented in Fig. 8. With increasing δ value, the chromaticity coordinates (x, y) of the phosphors vary systematically from (0.64, 0.36) to (0.58, 0.42), and the corresponding color tone changes gradually from orange-red to orange-yellow, which can meet the requirements for varying applications of white LEDs, such as desired color temperature and color point, as well as high luminous efficiency.

White LED lamps were fabricated by combining blue LED chips (450 nm) with $YAG:Ce^{3+}$ yellow-emitting phosphors or a blend of $YAG:Ce^{3+}$ and as-prepared $Ca_{0.98}Eu_{0.02}Al_{0.76}Si_{1.18}N_3$ phosphors. Figure 9 illustrates the electroluminescence spectra of the fabricated white LED lamps. By addition of the $Ca_{0.98}Eu_{0.02}Al_{0.76}Si_{1.18}N_3$ red-emitting phosphors, the red emission intensity around 650 nm is greatly improved and the FWHM of the emission spectrum expands obviously from ~120 to ~170 nm. Figure 10 displays the CRI values from $R1$ to $R8$ for white LED lamps fabricated by using only $YAG:Ce^{3+}$ or a blend of $YAG:Ce^{3+}$ and as-prepared $Ca_{0.98}Eu_{0.02}Al_{0.76}Si_{1.18}N_3$ phosphors. The general CRI value is designated by the symbol R_a, which is the average value of $R1$–$R8$. In comparison with the $YAG:Ce^{3+}$-based white LED, the white LED with addition of as-prepared red-emitting phosphor has higher values of $R1$–$R8$. The special CRI values from $R9$ to $R15$ are shown in Table III, which are not evaluated in calculating the general CRI value. We can see that all these CRI values increase a lot by adding as-prepared red-emitting phosphors to $YAG:Ce^{3+}$ yellow-emitting phosphors, which mean that the color of the objects can be precisely reproduced. Table IV summarizes the chromaticity coordinates, the CCTs, the general CRI values, and the luminous efficacies of the fabricated lamps with different mass ratios of $YAG:Ce^{3+}$ yellow-emitting and $Ca_{0.98}Eu_{0.02}Al_{0.76}Si_{1.18}N_3$ red-emitting phosphors. With the proportion of the red-emitting phosphor rising, the general CRI of the fabricated white LEDs increases from 71 to 91. At the same time, the CCT decreases from 5802 to 3500 K. The corresponding luminous efficacies drop slightly due to the self-absorption of yellow light by $Ca_{0.98}Eu_{0.02}Al_{0.76}Si_{1.18}N_3$ red-emitting phosphor and the reduction of lumen equivalent caused by peak wave length position shifting from about 550 to 630 nm.[33]

https://doi.org/10.1557/jmr.2015.125 Published online by Cambridge University Press

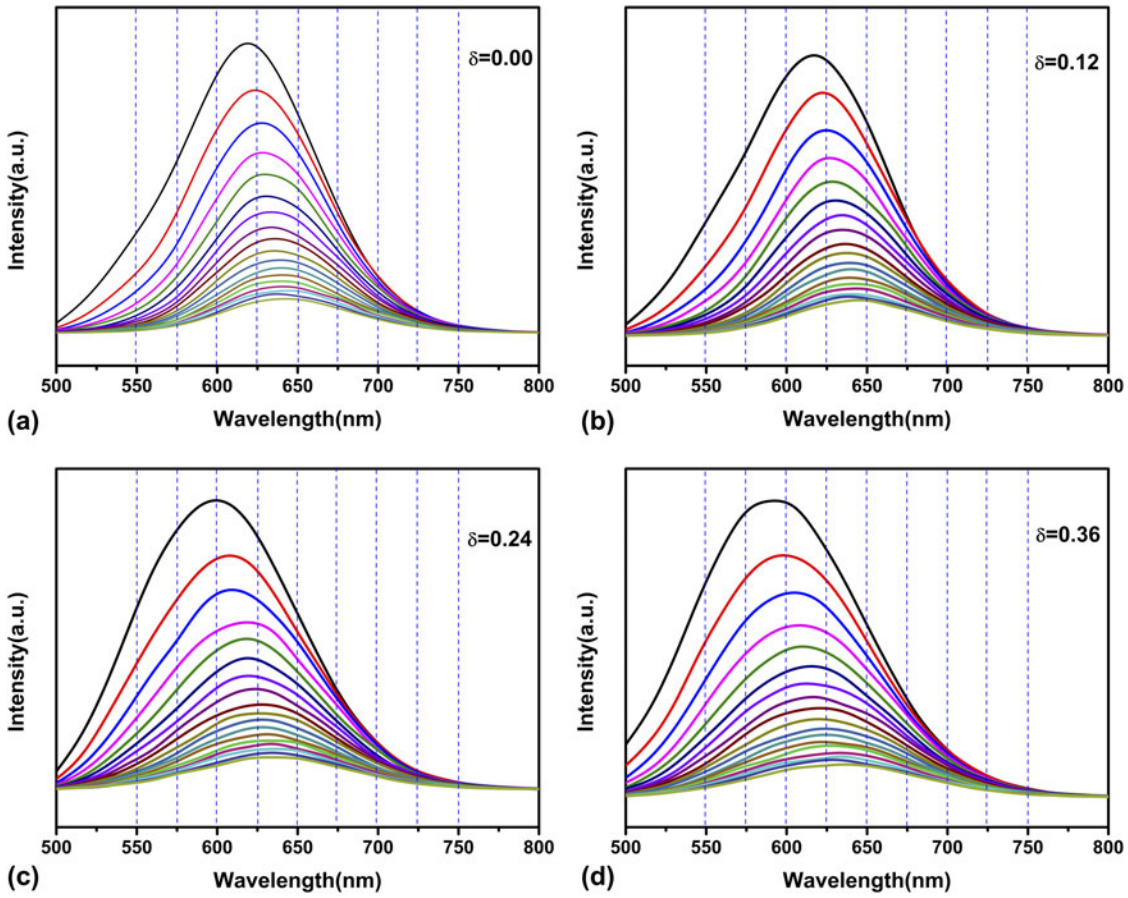


FIG. 7. TRPL spectra of $Ca_{0.98}Eu_{0.02}Al_{1-4\delta/3}Si_{1+\delta}N_3$ with δ = 0–0.36. The different colors represent different delay times for the TRPL curves, i.e., the black curve was acquired at a delay time of 100 ns, red at 200 ns, blue at 300 ns, and so on.

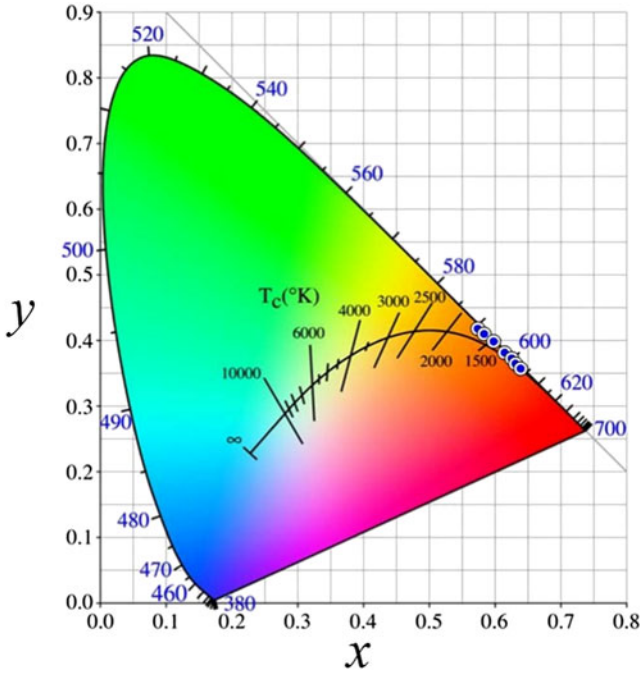


FIG. 8. CIE chromaticity diagram for $Ca_{0.98}Eu_{0.02}Al_{1-4\delta/3}Si_{1+\delta}N_3$ (δ = 0–0.36) phosphors excited at 460 nm.

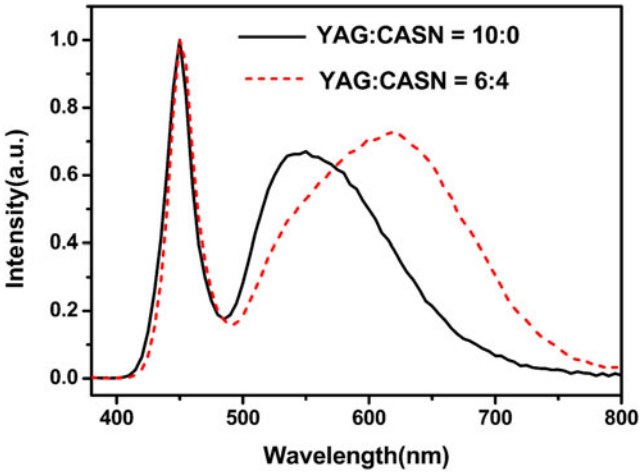


FIG. 9. Normalized electroluminescence spectra of the white LEDs fabricated by using $YAG:Ce^{3+}$ or $YAG:Ce^{3+}$ and as-prepared $Ca_{0.98}Eu_{0.02}Al_{0.76}Si_{1.18}N_3$ red-emitting phosphors combined with blue LED chips (450 nm).

https://doi.org/10.1557/jmr.2015.125 Published online by Cambridge University Press

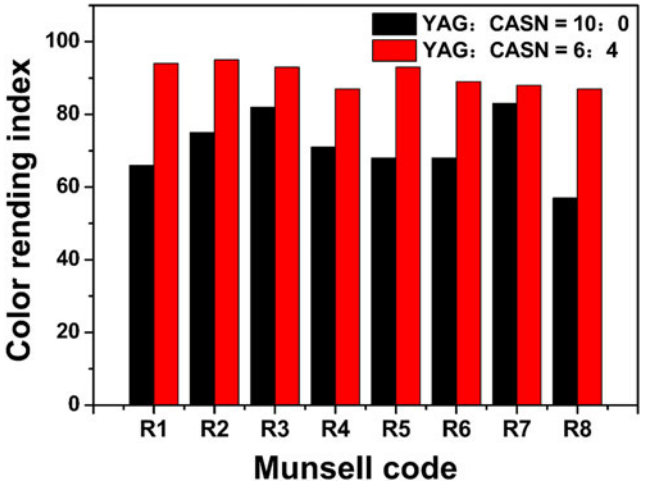


FIG. 10. CRI values from *R*1–*R*8 for white LED lamps fabricated by using $YAG:Ce^{3+}$ or blend of $YAG:Ce^{3+}$ and as-prepared $Ca_{0.98}Eu_{0.02}Al_{0.76}Si_{1.18}N_3$ red-emitting phosphors combined with blue LED chips (450 nm).

TABLE III. Special CRI values from *R*9 to *R*15 of the as-fabricated white LED lamps.

Phosphors used	*R*9	*R*10	*R*11	*R*12	*R*13	*R*14	*R*15
YAG:CASN = 10:0	0	42	67	41	68	90	60
YAG:CASN = 6:4	76	88	83	76	95	95	98

TABLE IV. Optical characteristics of white LEDs with different YAG/CASN ratios.

Phosphors used	CIE coordinates		CCT (K)	CRI (R_a)	Luminous efficacy (lm/W)
	x	*y*			
YAG:CASN = 10:0	0.3250	0.3593	5802	71	92
YAG:CASN = 8:2	0.3355	0.3177	5329	86	90
YAG:CASN = 7:3	0.3851	0.3560	3698	87	82
YAG:CASN = 6:4	0.3840	0.3338	3500	91	79

YAG refers to $YAG:Ce^{3+}$ and CASN refers to $Ca_{0.98}Eu_{0.02}Al_{0.76}Si_{1.18}N_3$.

IV. CONCLUSIONS

In summary, the nominal compositions of $Ca_{0.98}Eu_{0.02}Al_{1-4\delta/3}Si_{1+\delta}N_3$ (δ = 0–0.36) phosphors were synthesized by facile CTRN using stable and low-cost $CaCO_3$ as Ca source. The $CaAlSiN_3$-based phase without clear impurities was formed at a δ value of 0.18 with an external quantum efficiency of 71%. Blueshift emission was realized with increasing Si/Al molar ratio. There exist Si-rich and Si/Al-equivalent coordinated environments for Eu^{2+} ions in $Ca_{0.98}Eu_{0.02}Al_{1-4\delta/3}Si_{1+\delta}N_3$ phosphors. Energy transfer from high-energy component (Si-rich environment) to low-energy component (Si/Al-equivalent environment) has been confirmed by examining TRPL. The decay behaviors suggested that the energy transfer effect slowed with higher δ value. When combining a blend of $YAG:Ce^{3+}$ and as-prepared $Ca_{0.98}Eu_{0.02}Al_{0.76}Si_{1.18}N_3$ phosphors with a blue-emitting LED chip, warm white light LED can be generated with the general CRI of 91 at a low CCT of 3500 K.

ACKNOWLEDGMENTS

The authors are very grateful to the financial support from the National Natural Science Fund of China (No. 51172263, No. 51472087, and No. 11275249) and Shanghai Municipal Natural Science Foundation (No. 13ZR1412500).

REFERENCES

1. E-F. Schubert and J-K. Kim: Solid-state light sources getting smart. *Science* **308**, 1274 (2005).
2. T. Hashimoto, F. Wu, J-S. Speck, and S. Nakamura: A GaN bulk crystal with improved structural quality grown by the ammonothermal method. *Nat. Mater.* **6**, 568 (2007).
3. S. Pimputkar, J-S. Speck, S-P. DenBaars, S. Nakamura, and S. Nakamura: Prospects for LED lighting. *Nat. Photonics* **3**, 180 (2009).
4. R-J. Xie and N. Hirosaki: Silicon-based oxynitride and nitride phosphors for white LEDs—A review. *Sci. Technol. Adv. Mater.* **8**, 588 (2007).
5. R-J. Xie, N. Hirosaki, Y-Q. Li, and T. Takeda: Rare-earth activated nitride phosphors: Synthesis, luminescence and applications. *Materials* **3**, 3777 (2010).
6. R-J. Xie and H-T. Hintzen: Optical properties of (oxy)nitride materials: A review. *J. Am. Ceram. Soc.* **93**, 665 (2013).
7. R-J. Xie, N. Hirosaki, N. Kimura, K. Sakuma, and M. Mitomo: 2-phosphor-converted white light-emitting diodes using oxynitride/nitride phosphors. *Appl. Phys. Lett.* **90**, 191101 (2007).
8. X-Q. Piao, T. Horikawa, H. Hanzawa, and K. Machida: Characterization and luminescence properties of $Sr_2Si_5N_8:Eu^{2+}$ phosphor for white light-emitting-diode illumination. *Appl. Phys. Lett.* **88**, 161908 (2006).
9. X-Q. Piao, K. Machida, T. Horikawa, and H. Hanzawa: Self-propagating high temperature synthesis of yellow-emitting $Ba_2Si_5N_8:Eu^{2+}$ phosphors for white light-emitting diodes. *Appl. Phys. Lett.* **91**, 041908 (2007).
10. K-S. Sohn, S-J. Lee, R-J. Xie, and N. Hirosaki: Time-resolved photoluminescence analysis of two-peak emission behavior in $Sr_2Si_5N_8:Eu^{2+}$. *Appl. Phys. Lett.* **95**, 121903 (2009).
11. S-E. Brinkley, N. Pfaff, K-A. Denault, Z-J. Zhang, H-T. Hintzen, R. Seshadri, S. Nakamura, and S-P. DenBaars: Robust thermal performance of $Sr_2Si_5N_8:Eu^{2+}$: An efficient red emitting phosphor for light emitting diode based white lighting. *Appl. Phys. Lett.* **99**, 241106 (2011).
12. C-W. Yeh, W-T. Chen, R-S. Liu, S-F. Hu, H-S. Sheu, J-M. Chen, and H-T. Hintzen: Origin of thermal degradation of $Sr_{2-x}Si_5N_8:Eu_x$ phosphors in air for light-emitting diodes. *J. Am. Chem. Soc.* **134**, 14108 (2012).
13. O-M. ten Kate, Z. Zhang, P. Dorenbos, H-T. Hintzen, and E. van der Kolk: 4*f* and 5*d* energy levels of the divalent and trivalent lanthanide ions in $M_2Si_5N_8$ (M = Ca, Sr, Ba). *J. Solid State Chem.* **197**, 209 (2013).
14. T. Wang, P. Zheng, X-L. Liu, H-F. Chen, L. Bian, and Q-L. Liu: Effects of replacement of AlO^+ for SiN^+ on the structure and optical properties of $Sr_2Si_5N_8:Eu^{2+}$ phosphors. *J. Lumin.* **147**, 173 (2014).

https://doi.org/10.1557/jmr.2015.125 Published online by Cambridge University Press

15. K. Uheda, N. Hirosaki, and H. Yamamoto: Host lattice materials in the system Ca_3N_2-AlN-Si_3N_4 for white light emitting diode. *Phys. Status Solidi A* **203**, 2712 (2006).
16. J-W. Li, T. Watanabe, H. Wada, T. Setoyama, and M. Yoshimura: Low-temperature crystallization of Eu-doped red-emitting $CaAlSiN_3$ from alloy-derived ammonometallates. *Chem. Mater.* **19**, 3592 (2007).
17. X-Q. Piao, K. Machida, T. Horikawa, H. Hanzawa, Y. Shimomura, and N. Kijima: Preparation of $CaAlSiN_3:Eu^{2+}$ phosphors by the self-propagating high-temperature synthesis and their luminescent properties. *Chem. Mater.* **19**, 4592 (2007).
18. Y-Q. Li, N. Hirosaki, R-J. Xie, T. Takeda, and M. Mitomo: Yellow-orange-emitting $CaAlSiN_3:Ce^{3+}$ phosphor: Structure, photoluminescence, and application in white LEDs. *Chem. Mater.* **20**, 6704 (2008).
19. H. Watanabe, M. Imai, and N. Kijimaz: Nitridation of *AE*AlSi for production of *AE*$AlSiN_3:Eu^{2+}$ nitride phosphors (*AE* = Ca, Sr). *J. Am. Ceram. Soc.* **92**, 641 (2009).
20. Z-J. Zhang, O-M. ten Kate, A. Delsing, E. van der Kolk, P-H-L. Notten, P. Dorenbos, J-T. Zhao, and H-T. Hintzen: Photoluminescence properties and energy level locations of RE^{3+} (RE = Pr, Sm, Tb, Tb/Ce) in $CaAlSiN_3$ phosphors. *J. Mater. Chem.* **22**, 9813 (2012).
21. T. Suehiro, R-J. Xie, and N. Hirosaki: Gas-reduction-nitridation synthesis of $CaAlSiN_3:Eu^{2+}$ fine powder phosphors for solid-state lighting. *Ind. Eng. Chem. Res.* **53**, 2713 (2014).
22. P. Pust, V. Weiler, C. Hecht, A. Tücks, A.S. Wochnik, A-K. Henß, D. Wiechert, C. Scheu, P-J. Schmidt, and W. Schnick: Narrow-band red-emitting $Sr[LiAl_3N_4]:Eu^{2+}$ next-generation LED-phosphor material. *Nat. Mater.* **13**, 891 (2014).
23. H. Watanabe and N. Kijima: Crystal structure and luminescence properties of $Sr_xCa_{1-x}AlSiN_3:Eu^{2+}$ mixed nitride phosphors. *J. Alloys Compd.* **475**, 434 (2009).
24. T. Wang, J-J. Yang, Y. Mo, L. Bian, Z. Song, and Q-L. Liu: Synthesis, structure and tunable red emissions of $Ca(Al/Si)_2N_2(N_{1-x}O_x):Eu^{2+}$ prepared by alloy-nitridation method. *J. Lumin.* **137**, 173 (2013).
25. S-X. Li, X. Peng, X-J. Liu, and Z-R. Huang: Photoluminescence of $CaAlSiN_3:Eu^{2+}$-based fine red-emitting phosphors synthesized by carbothermal reduction and nitridation method. *Opt. Mater.* **38**, 242 (2014).
26. K. Uheda, H. Yamamoto, H. Yamane, W. Inami, K. Tsuda, Y. Yamamoto, and N. Hirosaki: An analysis of crystal structure of Ca-deficient oxonitridoaluminosilicate, $Ca_{0.88}Al_{0.91}Si_{1.09}N_{2.85}O_{0.15}$. *J. Ceram. Soc. Jpn.* **117**, 94 (2009).
27. M. Mikami, H. Watanabe, K. Uheda, and N. Kijima: Nitridoaluminosilicate $CaAlSiN_3$ and its derivatives - Theory and experiment. *Mater. Res. Soc. Symp. Proc.* **1040**, Q10-09 (2008).
28. Y. Shen, W-D. Zhuang, Y-H. Liu, H-Q. He, and T. He: Preparation and luminescence properties of Eu^{2+}-doped CASN-sinoite multiphase system for LED. *J. Rare Earths* **28**, 289 (2010).
29. S-S. Wang, W-T. Chen, Y. Li, J. Wang, H-S. Sheu, and R-S. Liu: Neighboring-cation substitution tuning of photoluminescence by remote-controlled activator in phosphor lattice. *J. Am. Chem. Soc.* **135**, 12504 (2013).
30. Y-W. Jung, B. Lee, S-P. Singh, and K-S. Sohn: Particle-swarm-optimization-assisted rate equation modeling of the two-peak emission behavior of non-stoichiometric $CaAl_xSi_{(7-3x)/4}N_3:Eu^{2+}$ phosphors. *Opt. Express* **18**, 17805 (2010).
31. C. Kulshreshtha, J-H. Kwak, Y-J. Park, and K-S. Sohn: Photoluminescent and decay behaviors of Mn^{2+} and Ce^{3+} coactivated $MgSiN_2$ phosphors for use in light-emitting-diode applications. *Opt. Lett.* **34**(6), 794 (2009).
32. T. Wang, P. Zheng, X-L. Liu, H-F. Chen, S-S. Yang, and Q.L. Liu: Decay behavior analysis of two-peak emission in $Ca(Al/Si)_2N_2(N_{1-x}O_x):Eu^{2+}$ Phosphors. *J. Electrochem. Soc.* **161** (1), H25 (2014).
33. X-J. Wang, G-H. Zhou, H-L. Zhang, H-L. Li, Z-J. Zhang, and Z. Sun: Luminescent properties of yellowish orange $Y_3Al_{5-x}Si_xO_{12-x}N_x$:Ce phosphors and their applications in warm white light-emitting diodes. *J. Alloys Compd.* **519**, 149 (2012).

https://doi.org/10.1557/jmr.2015.125 Published online by Cambridge University Press